Journal of Power Sources 195 (2010) 4322–4326

Contents lists available at ScienceDirect

Journal of Power Sources

journal homepage: www.elsevier.com/locate/jpowsour

Short communication

Synthesis of high power type $LiMn_{1.5}Ni_{0.5}O_4$ by optimizing its preparation conditions

Yanyan Sun, Yifu Yang*, Hui Zhan, Huixia Shao, Yunhong Zhou

College of Chemistry and Molecular Science, Wuhan University, Wuhan 430072, PR China

ARTICLE INFO

Article history:
Received 7 August 2009
Received in revised form 3 December 2009
Accepted 21 January 2010
Available online 25 January 2010

Keywords:
Lithium ion batteries
Cathode materials
Spinel
Power batteries
Rate capability

ABSTRACT

$LiMn_{1.5}Ni_{0.5}O_4$ has been synthesized by an ultrasonic-assisted sol–gel method. The precursor is heat treated at a series of temperatures from 650 °C to 1000 °C. The structure and physical–chemical properties of the as-prepared powder are investigated by powder X-ray diffraction (XRD), scanning electron microscopy (SEM), cyclic voltammetry (CV) thermal gravimetric and galvanostatic charge–discharge tests in detail. As temperature goes up, the particle size increases, the reactivity of the material in 4 V region becomes more obvious, the structure of the samples become more stable and it behaves optimal electrochemical properties as the material is heat treated at 850 °C. When it is used as cathode active material in a lithium battery, it delivers high initial capacity of 134.5 mAh g^{-1} (corresponding to 91.7% of the theoretical capacity), and high rate discharge capability, e.g., 133.4, 120.6, 111.4, 103.2 and 99.3 mAh g^{-1} as discharged at 0.5, 1, 5, 10 and 15 C (1 C = 148 mA g^{-1})-rates, respectively. It also shows satisfactory capacity retention even at high rate of 5 C, which is about 99.83% of the capacity retention per cycle.

1. Introduction

The growing demands of employing lithium-ion batteries for high-power applications, e.g., hybrid electric vehicle, have induced extensive research efforts worldwide. $LiMn_{1.5}Ni_{0.5}O_4$, as a cathode material candidate for 5 V cell, is of special interest because of its high specific capacity and dominant plateau at around 4.7 V [1]. It delivers a dominant potential plateau at around 4.7 V, resulting from the redox reaction of Ni^{2+}/Ni^{4+} couple accompanied by Li^+ ion extraction–insertion. It is known that when a lithium battery with $LiMn_2O_4$ as active cathode material suffered from progressive fade in capacity during charge–discharge cycling by reason of the Mn^{3+} dissolution in the electrolyte and the Jahn–Teller effect [2,3]. Comparing to $LiMn_2O_4$, the manganese element is tetravalent in the structure of $LiMn_{1.5}Ni_{0.5}O_4$, it has restrained its dissolution into the electrolyte effectively, and it also results in its high discharge specific capacity and excellent cycling stability [4–7].

Recently, the optimizations of $LiNi_{0.5}Mn_{1.5}O_4$ are made mainly from three aspects: cation-substitution, surface modification and newly synthetic method. The cation-substituted $LiMn_{1.5-y}Ni_{0.5-z}M_{y+z}O_4$ (M = Li, Mg, Fe, Co, and Zn) spinel oxides exhibited better cyclability and rate capability in the 5 V region compared to the unsubstituted $LiMn_{1.5}Ni_{0.5}O_4$ cathodes due to a smaller lattice parameter difference among the three cubic phases formed during the charge–discharge process [8]. The 5 V spinel cathode $LiMn_{1.42}Ni_{0.42}Co_{0.16}O_4$ modified with 2 wt % nanosize Al_2O_3, ZnO, Bi_2O_3, and $AlPO_4$ with more stable surface chemistry suppressed the development of SEI layer and thereby improved the electrochemical performances significantly compared to the bare $LiMn_{1.42}Ni_{0.42}Co_{0.16}O_4$ [9]. A nanometric $LiNi_{0.5}Mn_{1.5}O_4$ spinel prepared via a simple template-based method that uses PEG 400 as a sacrificial template showed excellent rate performance [6]. In this work, we have optimized the synthetic conditions of $LiNi_{0.5}Mn_{1.5}O_4$ by fetching ultrasonic in the synthesizing process, and the synthesized compound with particles size in micro scale shows high discharge capability and excellent rate performance. In addition, we have studied the electrochemical performance as a function of firing temperature and Mn^{3+} formation in the synthetic process.

2. Experimental

The $LiNi_{0.5}Mn_{1.5}O_4$ samples were obtained by an ultrasonic-assisted sol–gel method. Stoichiometric amounts of $Li(AC)\cdot 2H_2O$, $Mn(AC)_2\cdot 4H_2O$, $Ni(AC)_2\cdot 2H_2O$ with a cationic ratio of Li:Ni:Mn = 1.05:0.5:1.5 were dissolved in ultrapure water. An extra 5 mol% amount of lithium salt was added for the compensation of lithium evaporation during calcinations. The solution was poured slowly into the citric acid aqueous solution prepared with ultrapure water accompanied by ultrasonic oscillation. After oscillated for 40 min in a mini ultrasonic cleaner chamber (100 W, 40 kHZ), the solution was dried at 90 °C for 12 h to form a sol, then the sol was heated at 120 °C until a green dry gel was formed. Afterwards,

* Corresponding author. Tel.: +86 27 87218624; fax: +86 27 68754067.
E-mail address: yang-y-f1@vip.sina.com (Y. Yang).

0378-7753/$ – see front matter © 2010 Elsevier B.V. All rights reserved.
doi:10.1016/j.jpowsour.2010.01.039

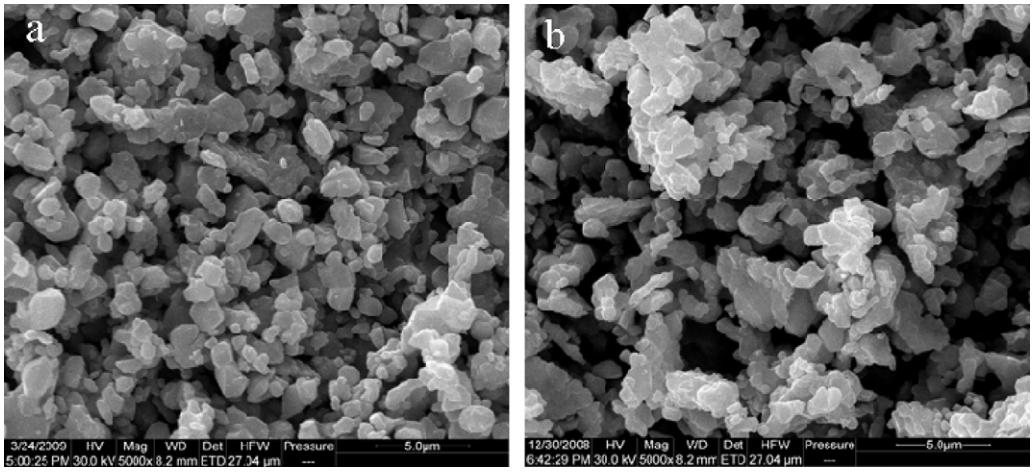

Fig. 1. Scanning electron micrographs of $LiNi_{0.5}Mn_{1.5}O_4$ synthesized by: (a) ultrasonic-assisted sol–gel method; (b) traditional sol–gel method.

the dried mass was heated at 400 °C for 4 h to make the organic compound to be decomposed absolutely, and then the temperature was raised to 650, 750, 850, 950 and 1000 °C and held for 10 h to obtain integrated crystalline samples. Accordingly the obtained materials are named as A650, A750, A850, A950, and A1000 in turn.

For evaluating the effects of ultrasonic on the performance of synthesized material, a comparing sample was also synthesized by traditional sol–gel method and it is named as B850. The preparation process for B850 was basically the same as that for A series samples except that the above-mentioned metal salt solution was poured slowly into the citric acid aqueous solution under constantly stirring until a sol formed. The whole process was conducted at 80 °C. The following parts are the same as the above steps, and the temperature for the second heat treatment was fixed at 850 °C.

Crystalline phase of the powder material was analyzed by powder X-ray diffraction (XRD-6000, Shimadzu, Japan) with Cu Kα radiation at the scanning speed of 0.5 min^{-1}. Surface images were characterized with scanning electron microscope (SEM, FEI Quanta 200, Holland). The thermal gravimetric analysis (TGA TA Q500) was employed for the analysis of the thermal stability of the materials. The precursor was heated at 500 °C for 15 h to remove the left organics.

Electrochemical properties of the powder materials were performed with coin cells (CR2016) using galvanostatic cycling, and with three-electrode cells for cyclic voltammogram tests. Positive electrode composites were prepared by 80 wt.% metal oxide powder, 15 wt.% acetylene black and 5 wt.% PTFE binder, the mixed materials were processed to form a membrane by a roller-presser, and finally the membrane was pressed into a piece of stainless steel meshes; the negative electrode was a metallic lithium, which also functioned as a reference electrode. The electrolyte was 1 M $LiPF_6$ in a 1:1 mixture of ethylene carbonate (EC)/dimethyl carbonate (DMC); the separator was Celgard 2300 membrane. The cells were assembled in an argon-filled glove box (Etelux LAB2000). The galvanostatic charge–discharge tests were performed at a charge rate of 0.2 C and different discharge rates between 3.5 and 5 V at 25 °C. The cyclic voltammetry experiments were carried out using a CHI605B Electrochemical Workstation (Chenhua instrument Ltd., Shanghai) under the same conditions as mentioned above.

3. Results and discussions

3.1. Comparison of the samples prepared with and without ultrasonic assistance

The difference between samples A850 and B850 is that, in the preparation process of the former one, ultrasonic oscillation was used instead of constantly stirring in the preparation of precursors. The scanning electron micrographs of A850 and B850 are shown in Fig. 1. It can be seen that although the particle size is almost the same for both samples, a worse agglomeration occurred in sample B850 and much narrower particle size distribution appeared in A850.

The initial discharge performances of these two samples were compared with the method of testing at 0.2 and 10 C, and the results are given in Fig. 2. At 0.2 C, the two samples show similar electrochemical behaviors to each other except that a little lower capacity and plateau are shown by B850. However, the rate performances of the two samples are quite different. In comparing, the sample A850 gives much higher specific capacity than B850 as it discharged at 10 C-rate, and gives a more than 200 mV higher discharge plateau than B850 which means that a larger polarization has happened at B850. So, we can obtain that the optimized method gives a superior rate performance for the material. Besides, the two samples all behave excellent cycling performance.

3.2. Physical properties analysis

The XRD patterns of A series samples of $LiMn_{1.5}Ni_{0.5}O_4$ powder heat treated at different temperatures are shown in Fig. 3. All fundamental diffraction peaks could be assigned to a nonstoichiometric cubic spinel structure with the space group of $Fd\bar{3}m$

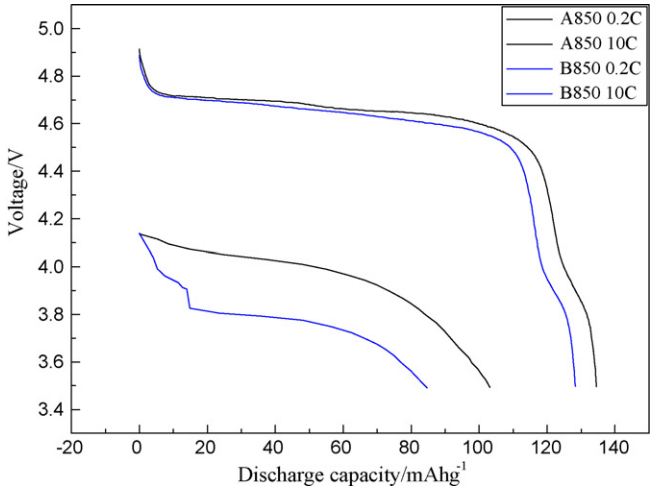

Fig. 2. Initial discharge curves of $LiNi_{0.5}Mn_{1.5}O_4$ synthesized by ultrasonic-assisted sol–gel method and traditional sol–gel method.

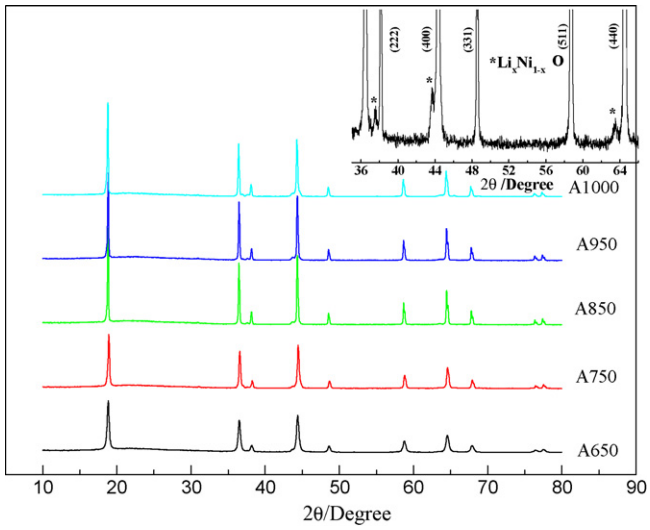

Fig. 3. Powder X-ray diffraction patterns of $LiNi_{0.5}Mn_{1.5}O_4$ annealed in air at various temperatures. The inset zooms in on the $Li_xNi_{1-x}O$ impurity.

[10]. By increasing the calcination temperature of the samples, sharper and higher diffraction peaks were observed, and thus, better crystalline structure of the $LiMn_{1.5}Ni_{0.5}O_4$ phase was obtained. However, it can be seen that the peaks observed at 37.5°, 43.7° and 63.6° (marked as asterisks in the inset of Fig. 3) were aroused from the weak impurity phase of $Li_xNi_{1-x}O$, this is consistent with the literature reports [5,6,11]. According to the previous report [11], the oxygen loss in samples heated above 650 °C can reduce the amount of Ni in the spinel phase, which causes the appearance of masses of Mn^{3+} ions to meet the demand of charge balance in spinel structure, and further results in the formation of a secondary phase and the appearance of a slight discharge plateau at 4.1 V, which will be discussed in the latter part. In order to get more evidence to support the analysis above, the thermal characteristics of

Table 1
Lattice parameters of the $LiNi_{0.5}Mn_{1.5}O_4$ samples heat treated at various temperatures.

Sample	Temperature (°C)	Lattice parameter (Å)
A650	650	8.1668
A750	750	8.1740
A850	850	8.1748
A950	950	8.1793
A1000	1000	8.1802

the precursor used for the preparation of A series samples were evaluated by thermogravimetric analysis, the result is not shown. And the onset temperature for oxygen loss is at 711.5 °C, which is consistent with the literature result [12] of 712 °C. Thus further heat treatment at higher temperature results in more serious oxygen deficiency, cation-disorder, and the occurrence of a second phase.

The lattice parameters obtained from Rietveld refinement based on a single phase of cubic spinel structure of the as-synthesized $LiMn_{1.5}Ni_{0.5}O_4$ powders heat treated at various temperatures are listed in Table 1. The lattice parameter a increases from 8.167 Å (corresponding to sample A650) to 8.180 Å (corresponding to sample A1000) as the treating temperature of the samples goes up. This result is because of that the radius of Mn^{3+} (0.65 Å) is larger than that of Mn^{4+} (0.53 Å) [13], then along with the temperature going up the oxygen loss in samples became more serious and more Mn^{3+} appears in samples treated at higher temperature.

The scanning electron micrographs of the precursor and final samples of A series samples of $LiMn_{1.5}Ni_{0.5}O_4$ heat treated at different temperatures are shown in Fig. 4. The grains of the samples A650 and A750 were not uniformly distributed and the sample A650 looks so much like the precursor except for smaller particle size. As reported in the literature, the significant crystallographic development occurred after the heat-treatment at 600 °C [14], so the integrated crystalloid did not form at low firing temperature. While as temperature was raised up, the particle shape becomes more uniform and the particle size becomes larger. As treated at

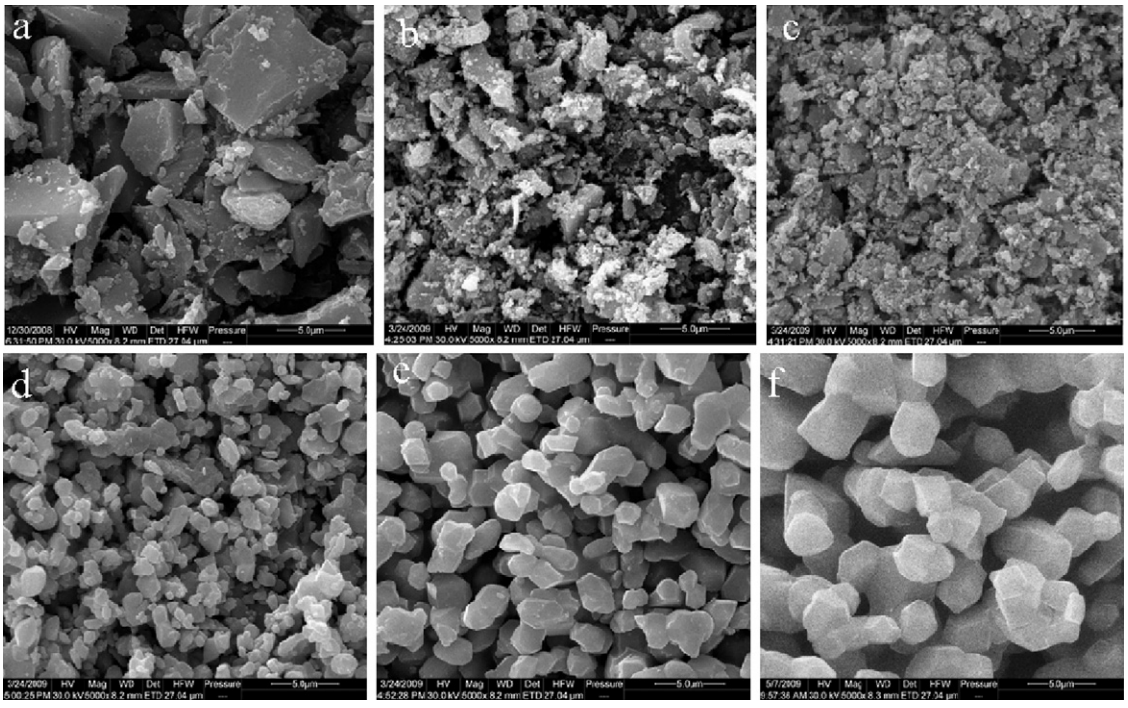

Fig. 4. Scanning electron micrographs of $LiNi_{0.5}Mn_{1.5}O_4$ heat treated at different temperatures: (a) synthesized precursor; (b) 650 °C; (c) 750 °C; (d) 850 °C; (e) 950 °C; (f) 1000 °C.

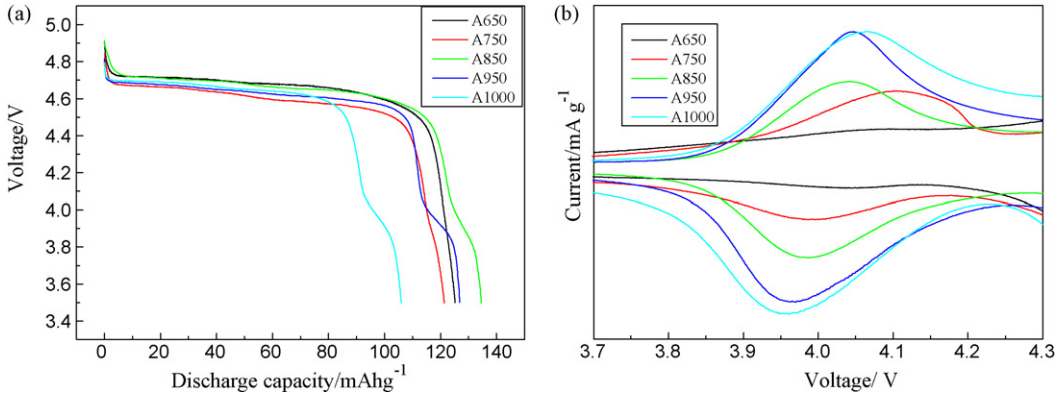

Fig. 5. (a) Initial discharge curves of $LiNi_{0.5}Mn_{1.5}O_4$ heat treated at different temperatures. The cells were charged at the rate of 0.2 C in voltage range of 3.5–5 V at 25 °C. (b) Cyclic voltammograms of $LiNi_{0.5}Mn_{1.5}O_4$ heat treated at different temperatures measured at a scan rate of 0.1 mV s^{-1}.

850 °C, the particles are well-distributed with little agglomeration and the size of the particles is between 0.5 and 2 μm (ca.).

3.3. Electrochemical properties

Fig. 5 shows the electrochemical properties of A series samples of $LiMn_{1.5}Ni_{0.5}O_4$ powder. The capacities in initial discharge vs. voltage curves at 0.2 C are shown in Fig. 5(a). They are 125.2, 121.3, 134.5, 126.8 and 106 mAh g^{-1} for A650, A750, A850, A950 and A1000, respectively. This can be ascribed that higher temperature gives birth to higher amount of $Li_xNi_{1-x}O$ and Mn^{3+} resulting in consuming the active Ni in the spinel, then the discharge capacity decreased when the treating temperature (T) is higher than 850 °C. While the integrated crystalline is not formed when T < 850 °C, the discharge capacities of A650 and A750 are lower than A850. Moreover, at around 4.7 V, there are two distinct reaction plateaus which correspond to Ni^{4+}/Ni^{3+} and Ni^{3+}/Ni^{2+} couples, respectively [15,16]. And yet an extra plateau appeared around 4 V when the treating temperature is higher than 750 °C and it becomes more obvious and flatter along with the increasing temperature. To get a deep understanding of the plateau around 4 V, cyclic voltammogram was tested between 3.5 and 5 V and the results between 3.7 and 4.3 V are shown in Fig. 5(b). The current peak becomes larger with increasing temperature. As is known, this extra plateau appeared around 4 V is due to the reaction of Mn^{3+}/Mn^{4+} redox couple [11,17,18], and as discussed in the forward part that the higher treating temperature gives birth to Mn^{3+} in the sample resulted from the oxygen loss. Therefore, this result could be explained as that oxygen-deficiency becomes more serious at higher treating temperature, as a result, larger number of Mn^{3+} come into existence.

In order to understand the distribution and changes in discharge capacity during the cycling process more clearly, the discharge processes were divided into two parts from 4.3 V. The released electric charge between 3.5 and 4.3 V was attributed to $Mn^{4+} \rightarrow Mn^{3+}$ reduction (marked as $Q1$) and the one above this voltage was attributed to $Ni^{4+} \rightarrow Ni^{2+}$ reduction (marked as $Q2$). The relation of the percentage (marked as P) of Q1 to the total ($Q1 + Q2$) and $Q1$ of $LiNi_{0.5}Mn_{1.5}O_4$ heat treated at different temperatures against the treating temperature is shown in Table 2. Along with the rising of the temperature, the percentage P increased linearly. The P and $Q1$ are the direct measurement of the amount of Mn^{3+}. In fact, the similar phenomenon has been found that the Cr-doped spinel show as much 4 V contributions from Mn^{3+} ions as expected from the composition [14]. Then it is the further evidence that larger number of Mn^{3+} come into existence at higher treating temperature.

Table 2
The 4 V region discharge capacities of $LiNi_{0.5}Mn_{1.5}O_4$ heat treated at different temperatures.

T (°C)	Discharge capacity (mAh g^{-1})		Percentage (%) (3.5–4.3 V)
	Total	3.5–4.3 V	
650	125.2	7	5.59
750	121.3	9.9	8.16
850	134.5	14.3	10.63
950	126.8	15.8	12.46
1000	106	16	15.09

To obtain the optimal synthesis temperature, the rate performances at 1 and 5 C are also tested and the detailed results are listed in Table 3. The discharge capacity at 10^{th} cycle was selected as the comparative standard just because the discharge capacity became stable after 10 cycles. It is found that the sample A850 gives the best electrochemical performance, such as the high initial discharge capacity and excellent capacity retention. As it has been reported that the diffusion coefficient of Li^+ ion in the reaction of $Mn^{4+} \rightarrow Mn^{3+}$ was higher than that in reaction of $Ni^{4+} \rightarrow Ni^{2+}$ [11] and the rate capability of the material was attributed to the presence of Mn^{3+}[19]. Then it is deduced that the increased high rate performance is associated with the increased amount of Mn^{3+}. As the treating temperature is higher than 850 °C, for the larger

Table 3
The rate performances of $LiNi_{0.5}Mn_{1.5}O_4$ heat treated at different temperatures.

T (°C)	Discharge capacity (mAh g^{-1})					
	1 C			5 C		
	10th	50th	Retention (%)	10th	50th	Retention (%)
650	111.4	96.1	86.27	96	80.6	83.94
750	99.4	83.5	84.00	86.2	72.4	83.99
850	117.2	116.4	99.32	112.4	104.6	92.53
950	106.8	98	91.76	74.4	51.8	69.62
1000	74.9	66.3	88.52	–	–	–

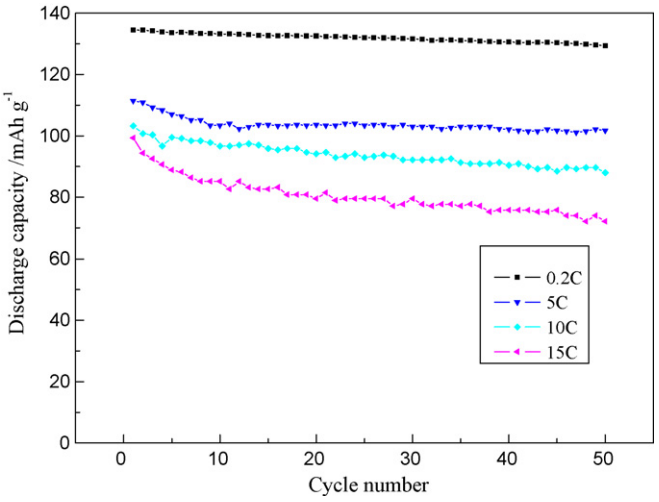

Fig. 6. Cycling performance of $LiNi_{0.5}Mn_{1.5}O_4$ heat treated at 850 °C. The cells were charged at the rate of 0.2 C and discharged at different rate in voltage range of 3.5–5 V at 25 °C.

particle size gives longer diffusion path of Li^+, the samples A950 and A1000 give worse electrochemical performance, especially for A1000. Therefore, we can obtain that the optimal synthesis temperature is 850 °C.

According to the above study, we give the detailed research and analysis of the electrochemical performance particular about the rate behaviors of the sample treated at 850 °C in the following part. The cycling performance of A850 is shown in Fig. 6. The rate behaviors of the sample A850 was measured at different discharge current densities from 30 mA g^{-1} (0.2 C) up to 2220 mA g^{-1} (15 C) with the same charge rate of 30 mA g^{-1} in the potential range of 3.5–5 V at 25 °C. At the discharge rate of 5, 10, 15 C, it delivers an initial discharge capacity of 111.4, 103.2, and 99.3 mAh g^{-1}, respectively. It can be observed that the sample A850 has very good capacity retention even at high discharge rates, e.g. the capacity retention of 99.83% per cycle can be reached even at 5 C-rate. Though a little fade of capacity is observed in the first 10 cycles, it keeps steady during the following cycles without further capacity decay. The excellent rate performance could be attributed by three factors. The first one is the effect of ultrasonic cavitations on the formation of the synthesized precursor. It could change the hydrolysis, condensation, nucleation and crystal growth processes [20]. On this basis, it may change the microstructure of the material and results in a more homogeneous distribution of Ni element in the lattice, which will further make the reaction that occurred in the charge–discharge process more thoroughly. The second one is the appropriate particle size distribution. Particle size has been shown to significantly influence the electrochemical activity of anodic and catholic materials. Larger particle size will enlarge the diffusion pass of Li^+ during the cycling and reduce the soakage of electrolyte in the materials, while smaller particle size with large specific surface area will give more chances to potential side reactions, such as Mn^{3+} dissolution in the electrolyte. The comparison of the structure stability and electrochemical behavior of nano- and micro-sized particles of spinel type $LiMn_{1.5}Ni_{0.5}O_4$, and the synergistic effect between nano and micro particles on the rate capabilities of spinel type $LiMn_{1.5}Ni_{0.5}O_4$ as cathode materials for Li-Ion batteries have been reported by Aurbach et al. and Morales et al., respectively [21,22]. The third one is the presence of Mn^{3+} which gives rise to the superior rate performance [20].

4. Conclusion

$LiNi_{0.5}Mn_{1.5}O_4$ material was synthesized by a simple ultrasonic-assisted sol–gel method, the physical and electrochemical performance was evaluated. According to the obtained results, following conclusion can be made:

(1) Ultrasonic-assisted sol–gel method has significant effect for the formation of more uniform particle size distribution and gives better electrochemical performance than the traditional method.
(2) The sample fired at 850 °C shows the best electrochemical performance, which delivers a high specific discharge capacity of 134.5 mAh g^{-1} at 0.2 C with a good cycling stability of 96.2% capacity retention after 50 cycles; shows high rate discharge capability. And it delivers amount of a specific discharge capacity of 99.3 mAh g^{-1} even at 15 C.
(3) With the increasing firing temperature, the oxygen-deficiency leads to the formation of $Li_xNi_{1-x}O$ impurity and an increasing content of Mn^{3+}, which is the result of the increasing specific capacity in the 4 V region.
(4) Since the method is simple and convenient for large-scale production and the material shows high discharge capability and excellent rate performance, it paves the way for practical use in lithium ion battery for high-power applications.

Acknowledgement

The financial support by the 863 National Research and Development Project Foundation of China (Grant no. 2006AA11A152) is gratefully acknowledged.

References

[1] M. Kunduraci, J.F. Al-Sharab, G.G. Amatucci, Chem. Mater. 18 (2006) 3585–3592.
[2] D.H. Jang, Y.J. Shin, S.M. Oh, J. Electrochem. Soc. 143 (1996) 2204–2211.
[3] Y. Xia, Y. Zhou, M. Yoshio, J. Electrochem. Soc. 144 (1997) 2593–2600.
[4] B. Markovsky, Y. Talyossef, G. Salitra, D. Aurbach, H. Kim, S. Choi, Electrochem. Commun. 6 (2004) 821–826.
[5] H.S. Fang, Z.X. Wang, B. Zhang, X.H. Li, G.S. Li, Electrochem. Commun. 9 (2007) 1077–1082.
[6] J.C. Arrebola, A. Caballero, M. Cruz, L. Hernán, J. Morales, E.R. Castellón, Adv. Funct. Mater. 16 (2006) 1904–1912.
[7] M. Kunduraci, G.G. Amatucci, Electrochim. Acta 53 (2008) 4193–4199.
[8] T.A. Arunkumar, A. Manthiram, Electrochem. Solid-State Lett. 8 (2005) A403–A405.
[9] J. Liu, A. Manthiram, Chem. Mater. 21 (2009) 1695–1707.
[10] J.H. Kim, S.-T. Myung, C.S. Yoon, S.G. Kang, Y.-K. Sun, Chem. Mater. 16 (2004) 906–914.
[11] Q. Zhong, A. Bonakdarpour, M. Zhang, Y. Gao, J.R. Dahn, J. Electrochem. Soc. 144 (1997) 205–213.
[12] M. Kunduraci, G.G. Amatucci, J. Electrochem. Soc. 153 (2006) A1345–A1352.
[13] S.H. Park, S.W. Oh, S.T. Myung, Y.C. Kang, Y.-K. Sun, Solid State Ionics 176 (2005) 481–486.
[14] S.H. Oh, S.H. Jeon, W.I. Cho, C.S. Kim, B.W. Cho, J. Alloys Compd. 452 (2008) 389–396.
[15] Y. Terada, K. Yasaka, F. Nishikawa, T. Konishi, M. Yoshio, I. Nakai, J. Solid State Chem. 156 (2001) 286–291.
[16] K. Dokko, M. Mohamedi, N. Anzue, T. Itoh, I. Uchida, J. Mater. Chem. 12 (2002) 3688–3693.
[17] K. Takahashi, M. Saitoh, M. Sano, M. Fujita, K. Kifunec, J. Electrochem. Soc. 151 (2004) A173–A177.
[18] K. Ariyoshi, Y. Iwakoshi, N. Nakayama, T. Ohzukua, J. Electrochem. Soc. 151 (2004) A296–A303.
[19] M. Kunduraci, G.G. Amatucci, J. Power Sources 165 (2007) 359–367.
[20] D. Chaumont, A. Craievich, J. Zarzycki, J. Non-Cryst. Solids 147–148 (1992) 41–46.
[21] Y. Talyosef, B. Markovsky, R. Lavi, G. Salitra, D. Aurbach, D. Kovacheva, M. Gorova, E. Zhecheva, R. Stoyanova, J. Electrochem. Soc. 154 (2007) A682–A691.
[22] J.C. Arrebola, A. Caballero, L. Hernán, J. Morales, Electrochem. Solid-State Lett. 8 (2005) A641–A645.